Int. J. Heat Mass Transfer. Vol. 36, No. 2, pp. 353–363, 1993
Printed in Great Britain

0017-9310/93 $6.00 + 0.00

A mathematical model for predicting the densification and growth of frost on a flat plate

Y.-X. TAO, R. W. BESANT and K. S. REZKALLAH
Department of Mechanical Engineering, University of Saskatchewan, Saskatoon, Saskatchewan S7N 0W0, Canada

(*Received* 17 *July* 1991 *and in final form* 6 *March* 1992)

Abstract—Frost deposition on a cold surface exposed to a warm moist air flow is simulated using a one-dimensional, transient formulation based on the local volume averaging technique. The spatial distribution of the temperature, ice-phase volume fraction (related to frost density), and rate of phase change within the frost layer are predicted. The time variation of the average frost density, frost thickness and heat flux at the cold surface shows a good agreement with the experimental data some distance downstream of the leading edge of a cold flat plate, providing that the proper transport properties are used. The results indicate that the local effective vapor mass diffusivity is up to seven times larger than the molecular diffusivity of water vapor in air as expressed by Fick's first law for frost temperatures between 264 and 272 K. This result is comparable with data measured for water vapor diffusion in snow.

1. INTRODUCTION

FROST formation on cold surfaces in heat exchanger applications has received attention since as early as 50 years ago. Two of the recent literature reviews [1, 2] summarize the large accumulation of frost growth literature. Both theoretical and experimental investigations have been carried out. However, despite a fairly large number of studies dealing with the frost formation process, little has been done to develop a rigorous mathematical model that can describe the dynamic process of frost deposition and internal frost densification. Until recently, the majority of models for a frost layer forming on a cold surface used simple models [2], in which only the average frost density, along the direction of frost growth, and frost surface temperature are predicted, i.e. no distributions of frost density and temperature within the frost layer are obtained. This is mainly due to the lack of sufficient knowledge of transport mechanism for frost densification within the frost layer and lack of sufficient experimental data confirming the trends of frost density and temperature distributions inside the frost layer. Sami and Duong [3] made an attempt to include the spatial variation of the frost density in their model. However, their formulation was somewhat implausible, and only the results of average frost density as a function of time were reported. In the early seventies, Brian and co-workers [4] found that their variable density model was unsuccessful in predicting the densification of the frost in the region near the cold surface. Their results showed that the frost density near the frost surface (warm side) is much higher than that near the cold side, which contradicts the experimental results reported by Cremers and Hahn [5]. It was speculated in ref. [4] that ice nuclei transport, under thermal diffusion, is the mechanism responsible for the internal densification of a frost layer, which is, as the authors acknowledged, not confirmed.

In this study, it is attempted to establish a mathematical model that can predict both spatial and temporal variation of the frost density and temperature. The frost thickness and the heat flux through the frost layer are also predicted. The analysis of frost structure by Hayashi *et al.* [6] provides a guideline to develop a model for frost formation during the initial period. A one-dimensional, transient heat and vapor diffusion formulation for porous media, using the local volume averaging technique, is then applied to the fully developed growth period of the frost layer. The appropriate boundary and initial conditions are specified for a typical forced convection problem over a flat plate. The results obtained numerically are compared with some newly acquired experimental data [7].

2. ANALYSIS

Frost growth on an initially clean cold surface can be divided into two periods: an early, relatively short, crystal growth period, and a fully developed frost layer growth period [6]. Due to structural differences, only in the fully developed growth period can the frost layer be modeled as a homogeneous (in a macroscopic sense) porous medium while, during the early crystal growth stage, convective heat and mass transfer over ice columns, rather than diffusion within the frost, is the main mechanism for frost growth. In the following, we first analyze the fully developed frost layer growth period, then present the model describing the early growth period.

NOMENCLATURE

a^* thermal diffusivity based on ice properties, $k^*_\beta/\rho^*_\beta c^*_{p\beta}$ [$m^2\ s^{-1}$]
a_0, a_1, a_2 empirical constants in equation (13)
Bi Biot number, $h^*\delta^*_0/k^*_{0,\text{eff}}$
Bi_m mass transfer Biot number, $h^*_m\delta^*_0/\alpha^*_{0,\text{eff}}$
c_p heat capacity at constant pressure
d diameter of the ice column
D^* vapor–air binary molecular diffusivity [$m^2\ s^{-1}$]
D_{eff} dimensionless diffusivity
D^*_0 diffusion coefficient [$m^2\ s^{-1}$]
F diffusion factor defined in equation (16)
Fo Fourier number, $\alpha^*_{0,\text{eff}}t^*/\delta^{*2}_0$
G functional defined in equation (11)
h^* film heat transfer coefficient [$W\ m^{-2}\ K^{-1}$]
h^*_m mass transfer coefficient [$m\ s^{-1}$]
h^*_{sg} enthalpy of sublimation [$J\ kg^{-1}$]
Ja Jacob number, $c^*_{p\beta}\Delta T^*/h^*_{sg}$
k thermal conductivity
l length scale for nucleation sites
Le Lewis number, α^*/D^*
$\dot{m}$ rate of phase change for water vapor
Nu_x Nusselt number, $h^*_t x/k^*_a$
p pressure
Q dimensionless heat flux
R^*_a air gas constant [$J\ kg^{-1}\ K^{-1}$]
Re_x Reynolds number, $u_\infty x/\nu$
R^*_v water vapor gas constant [$J\ kg^{-1}\ K^{-1}$]
Sh_x Sherwood number, $h^*_m x/D^*$
t time
T temperature
ΔT^* reference temperature difference, $T^*_\infty - T^*_c$ [K]
u_∞ ambient air velocity
W humidity ratio [$kg\ kg^{-1}$]
x coordinate axis parallel to air flow
z coordinate axis.

Greek symbols

α constant in equation (31)
$\alpha^*_{0,\text{eff}}$ effective thermal diffusivity, $k^*_{0,\text{eff}}/\rho^*_f c^*_p$ [$m^2\ s^{-1}$]
δ_f frost thickness
δ^*_0 reference length scale [m]
ε volume fraction
ρ density
τ tortuosity.

Subscripts

a air
c cold
f frost
s frost surface
t total
tp triple point
tr transition
v vapor phase
β ice phase
γ gas phase which consists of air and water vapor
0 initial; reference for non-dimensional scales (Table 1)
∞ ambient.

Superscripts

′ ratio
* dimensional.

2.1. *Fully developed frost layer growth* ($t > t_{tr}$)

A frost layer, during the fully developed growth stage, is treated as a porous medium with a distributed porosity and expanding boundary (Fig. 1(a)). The problem is formulated using the local volume averaging technique [8, 9]. The major assumptions used to arrive at the governing equations and boundary conditions are: (a) the transport of heat and mass in frost is macroscopically one dimensional; (b) the total pressure of the gaseous phase (water vapor plus air) in the ice matrix is constant; (c) local thermodynamic equilibrium exists, i.e. the gas phase temperature and solid (ice) temperature are the same; (d) gas-phase convection inside the frost layer is negligible compared with molecular diffusion; (e) the temperature dependence of the physical properties for individual phases is not considered; and (f) the gradient in the ice volume fraction at the boundaries of the frost layer is zero. Assumptions (b) and (c) are used for the purpose of simplification, and (d) is justified for one-dimensional problems. Assumption (e) leads to negligible errors of the computational results for the temperature ranges studied. Assumption (f) is consistent with the limited experimental data on frost density by Bong *et al.* [10], although more research work needs to be done.

2.1.1. *Governing equations.* For a spatial domain, $0 < z < \delta_f$, Fig. 1(a), the distributions of temperature, T, volume fraction of ice phase, ε_β, and volumetric rate of water vapor phase change, $\dot{m}$, can be described by the following, dimensionless governing equations:

energy equation

$$\rho_f c_p \frac{\partial T}{\partial t} + \dot{m}P_2 = \frac{\partial}{\partial z}\left(k_{\text{eff}}\frac{\partial T}{\partial z}\right); \qquad (1)$$

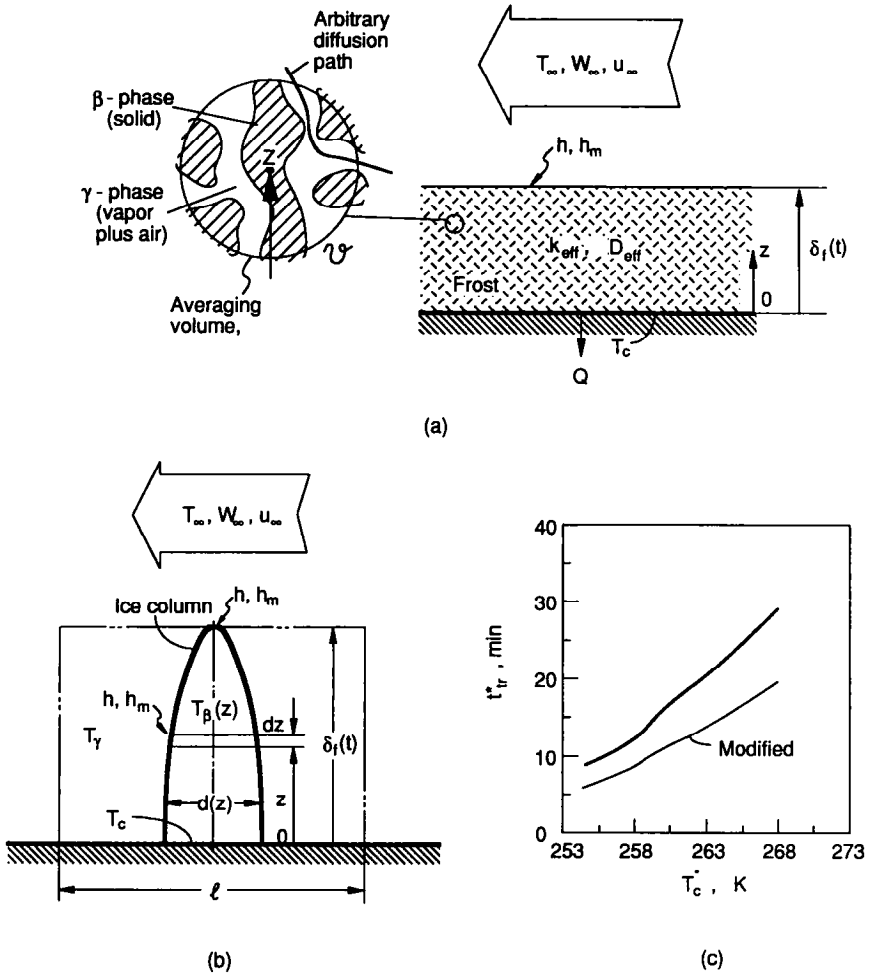

FIG. 1. Modeling of frost growth on a flat plate: (a) the local volume averaging formulation at the full growth period; (b) a unit cell for the ice column growth at the initial stage; and (c) the empirical relation between the transition time and the cold plate temperature [6] (the modification to t_{tr}^* shown is used to characterize the end of the ice column growth period).

ice phase continuity equation

$$\frac{\partial \varepsilon_\beta}{\partial t} + \frac{\dot{m}}{P_l} = 0; \tag{2}$$

gas diffusion equation

$$\frac{\partial(\varepsilon_\gamma \rho_v)}{\partial t} - \dot{m} = \frac{\partial}{\partial z}\left(D_{eff}\frac{\partial \rho_v}{\partial z}\right); \tag{3}$$

where the symbols are listed in Nomenclature, and the dimensionless variables and parameters are defined in Table 1. Except for ε_β and ε_γ, all the dependent variables are 'local volume averaged' or 'intrinsic phase averaged' [9]. The algebraic equations of constraint are:

volumetric constraint

$$\varepsilon_\beta + \varepsilon_\gamma = 1; \tag{4}$$

thermodynamic relations

$$p_a = p_t - p_v \tag{5}$$

$$p_a = P_3 \rho_a T \tag{6}$$

$$p_v = P_4 \rho_v T \tag{7}$$

and for the saturation condition

$$p_v = \exp\left[-P_5\left(\frac{1}{T} - \frac{1}{T_0}\right)\right]. \tag{8}$$

In the governing equations, the frost properties are defined as follows:

$$\rho_f = \varepsilon_\beta \rho_\beta + \varepsilon_\gamma(\rho_v + \rho_a) \tag{9}$$

$$c_p = \frac{\varepsilon_\beta \rho_\beta c_\beta + \varepsilon_\gamma(c_v \rho_v + c_a \rho_a)}{\rho_f} \tag{10}$$

$$k_{eff} = \varepsilon_\beta k_\beta + \varepsilon_\gamma \frac{k_v \rho_v + k_a \rho_a}{\rho_v + \rho_a} + (k_\beta - k_\gamma)G \tag{11}$$

$$D_{eff} = \frac{D^*_{v,eff}}{\alpha^*_{0,eff}} = \frac{\varepsilon_\gamma D^* + D^*_D}{\alpha^*_{0,eff}} \tag{12}$$

where G and D^*_D are derived from the thermal conductivity tensor and diffusivity tensor, respectively,

Table 1(a). Dimensionless variables

ρ	c_p	T	ρ_i	k_i	p_i	z	c_i	t	$\dot{m}$	δ_f	l	d
$\frac{\rho^*}{\rho_0^*}$	$\frac{c_p^*}{c_0^*}$	$\frac{T^*}{\Delta T^*}$	$\frac{\rho_i^*}{\rho_0^*}$	$\frac{k_i^*}{k_{0,\text{eff}}^*}$	$\frac{p_i^*}{p_{v,0}^*}$	$\frac{z^*}{\delta_0^*}$	$\frac{c_i^*}{c_0^*}$	$\frac{t^*}{\delta_0^{*2}/\alpha_{0,\text{eff}}^*}$	$\frac{\dot{m}^*}{\rho_0^*\alpha_{0,\text{eff}}^*/\delta_0^{*2}}$	$\frac{\delta_f^*}{\delta_0^*}$	$\frac{l^*}{\delta_0^*}$	$\frac{d^*}{\delta_0^*}$

Table 1(b). Dimensionless parameters

k_{eff}	D_{eff}	P_1	P_2	P_3	P_4	P_5
$\frac{k_{\text{eff}}^*}{k_{0,\text{eff}}^*}$	$\frac{D_{v,\text{eff}}^*}{\alpha_{0,\text{eff}}^*}$	$\frac{\rho_\beta^*}{\rho_0^*}$	$\frac{h_{sg}^*}{c_0^*\Delta T^*}$	$\frac{\Delta T^* R_v^* \rho_0}{p_{v,0}^*}$	$\frac{\Delta T^* R_a^* \rho_0}{p_{v,0}^*}$	$\frac{h_{sg}^*}{R_v^*\Delta T^*}$

which account for the non-homogeneity in pore structure at a microscopic level [8]. Using the definition of the frost density, equation (9), and treating all the properties for individual phases as constant (since $\rho_\beta \gg \rho_v + \rho_a$) and expressing G by a series expansion of ρ_f, equation (11) now becomes

$$k_{\text{eff}} = a_0 + a_1\rho_f + a_2\rho_f^2 + \cdots \tag{13}$$

where a_0, a_1, etc. may be treated as constants, although they are found to be a weak function of the cold plate temperature [11]. In many frost studies [1–3], an empirical relation, based on the average of the frost density over the entire frost layer with the form of equation (13) but truncated at the second power term, is recommended [11], i.e.

$$k_{\text{eff}}^* = 0.02422 + 7.214\times10^{-4}\rho_f^* + 1.1797\times10^{-6}\rho_f^{*2} \tag{14}$$

where the dimension for the frost density is kg m^{-3}, and that for the thermal conductivity is W m^{-1} K^{-1}. The reader is referred to Yen [12] for additional empirical equations for the thermal conductivity of snow. Equation (14) is employed in our calculation.

Similar to G, the second vapor mass diffusivity, D_D^*, in equation (12) arises due to the lateral or three-dimensional diffusion (microscopic phenomenon) of water vapor in a frost layer that is modeled as one dimensional (macroscopic description). According to ref. [8], D_D^* is a strong function of ε_γ. As a first degree approximation, we define

$$D_D^* = F\varepsilon_\gamma D^* \tag{15}$$

where F may be called the 'diffusion factor'. Thus, the effective vapor diffusivity in equation (12) becomes

$$D_{v,\text{eff}}^* = \varepsilon_\gamma D^*(1+F). \tag{16}$$

The diffusion factor, F, includes several physical effects: the combined ordinary (or bulk) and Knudsen diffusion, metamorphism within the frost structure [12], pore-size distribution (irregular shape and tortuous diffusion path) and variation of gaseous pressure within fine pores (instead of a constant pressure). Knudsen diffusion, which results in diffusion rates higher than water vapor in air, occurs when the pore size is of the same order as the mean free path of molecules. This may be important when diffusion within the crystal structure becomes dominant as the frost density increases [13], i.e. no fluid flow occurs within frost. More research is needed to quantify this complex phenomenon. Unlike in the case of k_{eff}, there is no empirical relation available to evaluate, $D_{v,\text{eff}}^*$ or F. Some measurements of water vapor diffusion in snow suggest that F should have a value of about three to four [12, 14]. For simplicity, F is treated as a constant within the frost layer ($0 < z < \delta_f$) and F_s is specified at $z = \delta_f$. In the discussion section, the influence of F on frost densification will be investigated, and experimental data on average frost density and thickness [7] will be used to determine F and F_s indirectly.

In the above formulation, the unknown variables are T, ρ_v, ρ_a, ε_β, ε_γ, $\dot{m}$, p_a and p_v while all the transport and thermophysical properties for the individual phases are known from empirical data. Equations (3)–(10) can then be used to solve for these eight unknowns providing that the thickness of the frost domain, δ_f, and other boundary and initial conditions are specified.

2.1.2. *Boundary conditions.* At the frost surface, we have

$$Bi_m[W_\infty - W(z=\delta_f,t)] = D_{\text{eff,s}}\frac{\partial\rho_v(z=\delta_f,t)}{\partial z} + \rho_f\frac{d\delta_f}{dt} \tag{17}$$

where

$$W = 0.6218\frac{p_v}{p_t - p_v} \tag{18}$$

$$Bi[T_\infty - T(z=\delta_f,t)] = k_{\text{eff}}\frac{\partial T(z=\delta_f,t)}{\partial z} - P_2\rho_f\frac{d\delta_f}{dt} \tag{19}$$

$$\frac{\partial\varepsilon_\beta(z=\delta_f,t)}{\partial z} = 0. \tag{20}$$

Equations (17), (19) and (20) yield δ_f, $T(z = \delta_f)$ and $\varepsilon_\beta(z = \delta_f)$. If, in calculation, the frost surface temperature becomes 0°C, equation (19) is then used to find δ_f by assuming that when the surface temperature reaches 0°C, heat transfer rather than mass transfer on the surface governs the rate of frost growth. Thus, equation (17) can be used to evaluate the actual mass transfer coefficient, h_m^*. This assumption implies the inclusion of a melting phenomenon if the heat of evaporation instead of the heat of sublimation is used in equation (19).

At the cold plate surface, we have

$$T(z = 0, t) = T_c \tag{21}$$

$$\frac{\partial \varepsilon_\beta(z = 0, t)}{\partial z} = 0. \tag{22}$$

The film heat transfer coefficient between the ambient convective flow and the frost surface is known to be different from that between the ambient flow and a smooth surface [1], and the mass transfer coefficient is not always analogous to the heat transfer coefficient because of roughness effects [15]. A number of empirical correlations for frost surface heat and mass transfer coefficients have been reported for various test conditions [1–4, 6, 7]. In order to compare our prediction with the experimental data presented in ref. [7], as will be seen later, the following correlations for Nu_x and Sh_x are used in this study (also see Appendix)

$$Nu_x = 0.720\left(\frac{x}{d_H}\right)^{0.698} W_\infty^{0.294} T'^{0.729}\, Re_{d_H}^{0.721}\, Fo_{d_H}^{0.036} \tag{23}$$

$$Sh_x = 1.019\times 10^{-5}\left(\frac{x}{d_H}\right)^{0.781} W_\infty^{-2.859} T'^{-0.119} \times Re_{d_H}^{0.185}\, Fo_{d_H}^{-0.187}. \tag{24}$$

The Nusselt number given in the above equation is based on the overall heat transfer coefficient, h_t^*. The air–frost film heat transfer coefficient should be

$$h^* = h_t^* - \frac{\dot{m}''^* h_{sg}^*}{T_a^* - T_{tp}^*} \tag{25}$$

where $\dot{m}''^* = \delta_f^* \rho_f^*$ is the frost mass concentration flux determined using the correlations listed in the Appendix. The initial conditions for the frost layer growth problem, i.e. the distributions of T, ρ_v and ε_β at $t = t_{tr}$, are taken from the solutions of the early crystal growth model, as will be discussed below.

A length scale, δ_0^*, is used to normalize the variables (Table 1), and is defined as the frost thickness when the frost surface temperature reaches the triple point temperature and the growth rate equals zero. From equation (17), if we put $d\delta_f/dt$ equal to zero, this asymptotic frost thickness is

Table 2. Reference data for δ_0^*

T_{a0}^*	[K]	293
T_{c0}^*	[K]	263
h_{m0}^*	[kg m^{-2} s^{-1}]	9.5×10^{-3}
Re_{x0}		7.8×10^{4}
F_{s0}		0.52
k'		1.1
$\varepsilon_{\gamma 0}$		0.8

$$\delta_0^* = \frac{\bar{D}_{eff,0}^* \dfrac{d\rho_v^*}{dT^*} k'(T_{tp}^* - T_{c0}^*)}{h_{m0}^*(W_a - W_s)} \tag{26}$$

where $\bar{D}_{eff,0}^*$ is the time averaged effective mass diffusivity, W_s is the humidity ratio at the frost surface and evaluated at T_{tp}^*, and k' is the ratio of the average effective thermal conductivity of the frost layer to the frost surface thermal conductivity. The above-defined reference length scale allows us to evaluate the magnitude of the frost thickness with respect to time and also to compare the thermal diffusion time scale $(\delta_0^{*2}/\alpha_{0,eff}^*)$ with the deposition time. The reference values, to determine the length scale for the examples calculated in this study, are listed in Table 2.

2.2. *Ice column growth* $(0 < t < t_{tr})$

During the early stage of frost formation, ice columns grow at the sites where subcooled-liquid nucleation occurs [11], i.e. the continuous matrix has not been formed. The local thermodynamic equilibrium is no longer applicable to both the ice phase and gaseous phase adjacent to these ice columns. We postulate a growing-circular-fin model of the ice column, as shown in Fig. 1(b), to simulate the crystal growth. It is assumed that the temperature distribution of the ice column is one dimensional, the side-wise heat transfer coefficient is the same as that from the ambient, and the effect of thermal boundary layer due to the ambient convective flow is included in the specification of the gaseous phase temperature, T_γ (Fig. 1(b)), which has a value between the ambient and cold plate temperatures. Although the model assumed for this early stage of frost growth is consistent with the observations of Hayashi *et al.* [6], the model is perhaps overly simplistic and may not exactly model all the physical phenomena. This model is thought to be of secondary interest while the fully developed frost growth is of primary interest.

The dimensionless energy equation and mass balance equation for the ice column in Fig. 1(b) are

$$d\frac{\partial T_\beta}{\partial t} = d\frac{\partial^2 T_\beta}{\partial z^2} + 2\frac{\partial T_\beta}{\partial z}\frac{\partial d}{\partial z} - 4Bi_\beta(T_\beta - T_\gamma) + \frac{2}{Ja}\frac{\partial d}{\partial t} \tag{27}$$

$$\frac{\partial d}{\partial t} = 2Bi_{m\beta}(W_\gamma - W) \tag{28}$$

where W is evaluated at $T_\beta(z, t)$ using equation (18),

and W_γ is evaluated at T_γ. T_γ is a constant and is found from the following approximation:

$$T_\gamma = \alpha T_\infty + (1-\alpha)T_c \quad (29)$$

where $0 < \alpha < 1$ depending on the ambient thermal boundary layer thickness. The parameter α will be larger for turbulent flow than that for laminar flow. The precise determination of T_γ requires knowledge of fluid mechanics coupled with heat and mass transfer around the ice columns (the surface roughness effect). Using the approximation (29) simplifies the formulation but still includes the non-equilibrium effect between the ice temperature and adjacent air temperature. (The selected value of α, for the example results presented later, is listed in Table 3.) The variables in the above equations are normalized with the same scales as listed in Table 1, except for the following quantities:

$$Bi_\beta = \frac{h^*\delta_0^*}{k_\beta^*}, \quad Ja = \frac{c_{p\beta}^*\Delta T^*}{h_{sg}^*}, \quad t = \frac{t^*}{\delta_0^{*2}/a^*}$$

$$a^* = \frac{k_\beta^*}{\rho_\beta^* c_{p\beta}^*}, \quad Bi_{m\beta} = \frac{h_m^*\delta_0^* c_{p\beta}^*}{k_\beta^*}.$$

The boundary conditions are

$$\frac{d\delta_f}{dt} = Bi_{m\beta}[W_\infty - W(z=\delta_f)] \quad (30)$$

$$T(z=0,t) = T_c \quad (31)$$

$$\frac{\partial T(z=\delta_f,t)}{\partial z} = Bi_\beta[T_\infty - T(z=\delta_f,t)] + \frac{1}{Ja}\frac{d\delta_f}{dt} \quad (32)$$

$$\frac{\partial d(z=0,t)}{\partial z} = 0 \quad (33)$$

$$d(z=\delta_f,t) = d_0. \quad (34)$$

In addition, it is assumed that the same film heat transfer coefficient applied to the entire ice surface, and the following equation, based on the thermal boundary layer theory [16], is used

Table 3. Selected parameters used in numerical examples

T_c^*	[K]	253 (263)†
T_∞^*	[K]	293
W_∞	[kg kg^{-1}]	8.854×10^{-3}
d_{H}	[m]	0.0375
l^*	[m]	5×10^{-4}
d_0^*	[m]	10^{-4}
δ_{f0}^*	[m]	10^{-4}
x^*	[m]	0.3
δ_0^*	[m]	2.9×10^{-3}
ρ_0^*	[kg m^{-3}]	92.84‡
$k_{0,eff}^*$	[W m^{-1} K^{-1}]	0.245‡
α		0.4
$\alpha_{0,eff}^*$	[m^2 s^{-1}]	1.38×10^{-6}
t_{tr}^*	[s]	240 (800)
Re_x		3.94×10^4 (3.87×10^4)
F		0.11 (3)
F_s		−0.9 (−0.33)

† The value in parentheses corresponds to $T_c^* = 263$ K.
‡ The reference $\varepsilon_{\beta 0} = 0.1$.

$$Nu_x = 0.03 Re_x^{0.8} Pr^{0.6}. \quad (35)$$

The mass transfer coefficient is found based on heat and mass transfer analogy [17]

$$h_m^* = \frac{h^*}{c_p^* Le^{2/3}}. \quad (36)$$

The initial conditions for the ice column growth period are assumed to be

$$\delta_f(t=0) = \delta_{f0} \quad (37)$$

$$d(z, t=0) = d_0 \quad (38)$$

$$T(z, t=0) = T_c. \quad (39)$$

It is implied that at time $t = 0$ small ice particles are distributed uniformly over the plate at a large number of nucleation points.

It is reported in an experimental study [6] that the transition time, characterizing the end of the crystal growth period, depends on the cold plate temperature, as shown in Fig. 1(c). Note that the above circular-fin approximation for the ice column growth does not lead to any dendritic frost growth near the end of the so-defined crystal growth period described in ref. [6]. Therefore, the transition time in the present study would be shorter than that obtained from experimental observations by ref. [6]. Guided also by the comparison of our calculation with the experimentally measured average density data [7] (as will be discussed further below), we modify the transition time in the calculation, t_{tr}, to be 2/3 of that reported by ref. [6] (see the second line in Fig. 1(c)). With this modification, the dendritic frost growth is considered to be a part of the full growth period of frost.

The average density of the frost layer at a given time is calculated from the following equations:

ice column growth period

$$\bar{\rho}_f(t) = \frac{\int_0^{\delta_f}\left[\frac{\pi}{4}d^2\rho_\beta + \left(l^2 - \frac{\pi}{4}d^2\right)(\rho_a + \rho_v)\right]dz}{l^2\delta_f}; \quad (40)$$

frost layer growth period

$$\bar{\rho}_f(t) = \frac{1}{\delta_f}\int_0^{\delta_f}\rho_f(z,t)\,dz. \quad (41)$$

At the transition time, the local average temperature is calculated as follows:

$$T(z, t=t_{tr}) = \varepsilon_\beta T_\beta(z, t=t_{tr}) + (1-\varepsilon_\beta)T_\gamma \quad (42)$$

where $\varepsilon_\beta = \pi d^2/(4l^2)$. In order to evaluate the effect of frost growth on heat transfer through the cold plate, a dimensionless heat flux, $Q = Q_k^*/Q_h^*$, is defined where Q_k^* is the heat flux conducted from the frost to the cold plate and $Q_h^* = h^*(T_\infty^* - T_c^*)$ is the convection heat flux from the ambient to the cold plate without the frost formation:

ice column growth period

$$Q = 1 + \left(\frac{k_\beta}{Bi_\beta}\frac{\partial T(z=0,t)}{\partial z} - 1\right)\frac{\pi}{4}\left(\frac{d}{l}\right)^2 \quad (43)$$

frost layer growth period

$$Q = \frac{k_{\text{eff}}}{Bi}\frac{\partial T(z=0,t)}{\partial z}. \quad (44)$$

It should be noted that the initial values of δ_{f0}, d_0 and l are related to the subcooling process of condensed water vapor; therefore, they depend on the material used for the cold plate, degree of subcooling and ambient conditions. The experimental determination of this relation under subfreezing conditions is important. In this study, these data are selected based on the average values in drop-wise condensation applications [18] (see also Table 3).

2.3. *Computational procedure*

The finite difference forms of equations (1)–(3), (27) and (28) are derived using the upwind difference scheme for the time derivative, the central difference scheme for internal nodes, and the backward, or forward, difference scheme for the boundary nodes. A downwind first-order difference scheme is used for the frost growth rate, equations (17) and (30), to achieve stability. Equation (17) (or (30) for the early stage) then gives the frost thickness for the next time step. If the frost surface temperature, $T(z = \delta_f)$, reaches the triple point temperature, equation (19) is used to find δ_f for the next time step. Equations (1)–(3) yield T, ε_β and $\dot{m}$, and the vapor density is found from Clapeyron equation (8). The relaxation iteration scheme is used to solve for the difference equations. The results are considered to be convergent when the deviation of any variable from the last iterated value is within 10^{-4}%.

The number of the grids in the frost domain is fixed. Therefore, for each time step, the spatial coordinates are updated based on the new boundary position, δ_f. The spatial distribution of each variable at the last time step is also updated to fit the new coordinate system, using a cubic spline polynomial interpolation method. To minimize the errors introduced by interpolation, a small time step of 1 s is chosen in the calculations. The spatial grid number of 10 is used; increasing the grid number to 20 shows a negligible difference in the results. A typical computation for a 2 h frost formation process takes about 4.3 cpu min on a medium-speed main frame computer.

3. RESULTS AND DISCUSSION

3.1. *Initial frost formation*

Calculations are performed for the typical frosting conditions listed in Table 3. The typical distributions of the ice column diameter and the temperature along the ice column are shown in Fig. 2. It can be seen that the ice column diameter at the frost surface ($z = \delta_f$) is less than that at the cold plate surface ($z = 0$). This distribution in d, although directly resulting from the specification of the boundary condition at $z = \delta_f$ (i.e. $d(z = \delta_f) = d_0$), is much closer to the experimental observation [6]. As will be discussed below, the trend in the frost density distribution during the full-frost-layer growth period largely depends on the distribution in ε_β at $t = t_{tr}$. In Fig. 2(b), it is shown that the temperature distribution in the ice column is relatively steady, compared with the strong variation in d with time. In general, the temperature of the ice column is very close to the cold plate temperature (for example, shown in Fig. 2(b), $T^* - T_c^* < 1$°C).

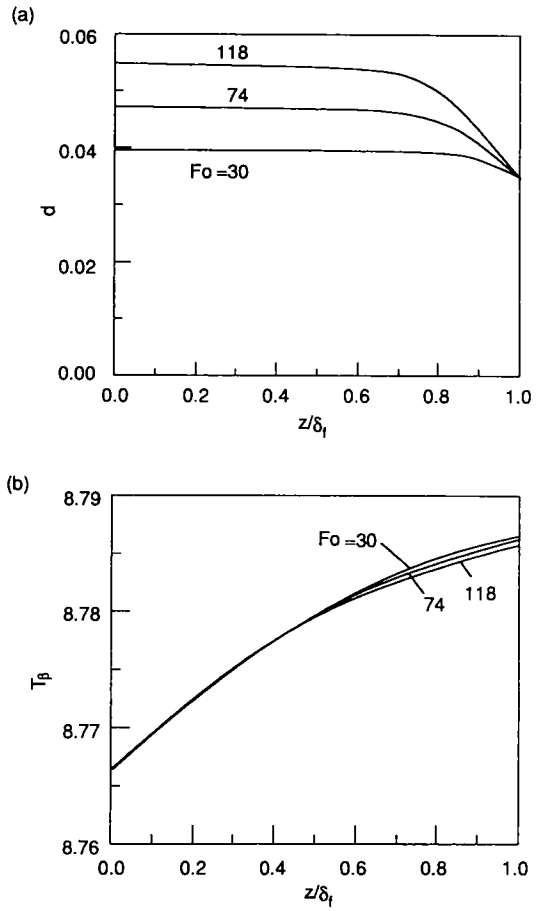

FIG. 2. Spatial distributions of (a) the ice column diameter; and (b) temperature: $T_c^* = 263$ K (the other conditions are listed in Table 3).

3.2. *Frost layer growth*

Figure 3 presents the typical distributions of four important variables within the frost layer for various Fourier numbers. Both temperature and vapor density show a non-linear distribution within the frost layer (although the non-linearity for the temperature is less significant than that for the vapor density, Figs. 3(a) and (b)). The non-linearity in the vapor density

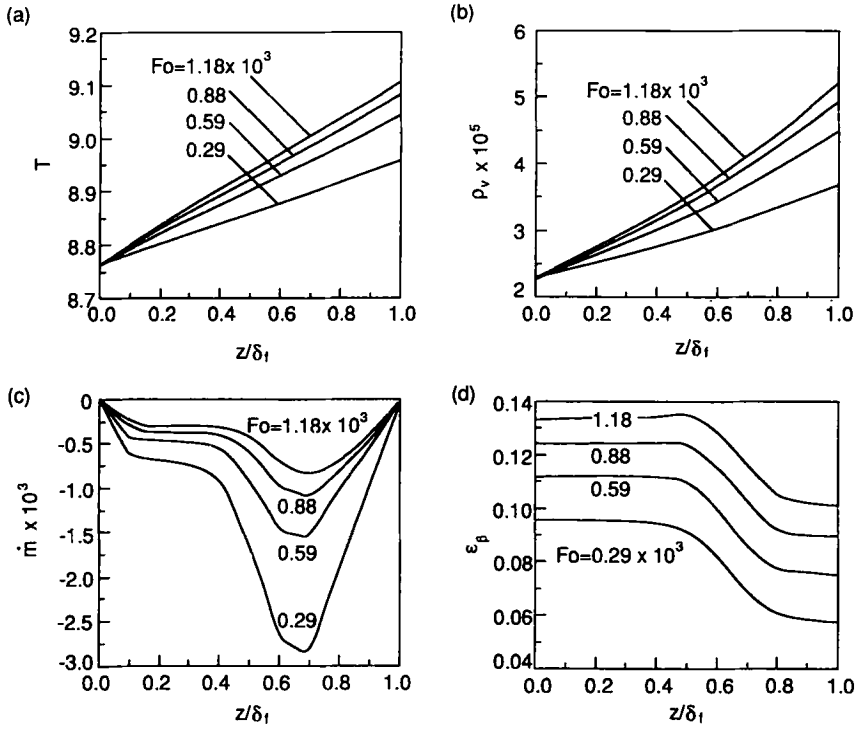

FIG. 3. Spatial distributions of (a) T, (b) ρ_v, (c) $\dot{m}$, and (d) ε_β for various Fo: $T_c^* = 263$ K.

results in a negative rate of phase change, $\dot{m}$ (Fig. 3(c), also see equation (5)), meaning that water changes from its gaseous phase into the solid phase [8]. According to the continuity equation for the ice phase, equation (2), ε_β then increases with time, as shown in Fig. 3(d). It is interesting to see that the mass rate of phase change per unit volume, $\dot{m}$ (which is the rate of densification), has a maximum absolute value near the frost–air interface, the warm side of the frost layer. This trend leads to frost in that region densifying faster than that at the region close to the cold plate. As shown in Fig. 3(d), the curve of ε_β at $Fo = 1180$ is flatter than that at $Fo = 290$. The results are consistent with the experimental data on the frost density distribution, reported in ref. [5]. In that work, it was found that during the initial period the frost density is higher near the cold side, while after a longer period of time, the frost density near the warm side becomes larger. However, caution must be taken in making a qualitative comparison between two studies since the data in ref. [5] are very limited. Nevertheless, the above-mentioned results lead to the following two observations:

(i) The frost density distribution in the full growth period largely depends on its distribution during the early growth period; and

(ii) The maximum densification rate occurs near the warm side of the frost layer.

As shown in Fig. 4, the temperature, T_s, no longer significantly increases with time after Fo reaches a certain value. During the quasi-steady-state period after $Fo = Fo_{ss}$, the temperature and vapor density can be represented by the following expressions

$$T(Fo \geqslant Fo_{ss}) = T(z/\delta_f, Fo = Fo_{ss})$$

$$\rho_v(Fo \geqslant Fo_{ss}) = \rho_v(z/\delta_f, Fo = Fo_{ss})$$

where $0 \leqslant z \leqslant \delta_f$. As seen in Fig. 4, Fo_{ss} increases as the cold plate temperature, T_c, increases. In general, Fo_{ss} is also strongly related to the ambient air humidity ratio and temperature.

In Fig. 4, the time variation of the dimensionless heat flux, Q, is also shown. For $T_c^* = 263$ K, Q, during the early growth period, increases with time, indicating the strong fin-effects. As the frost layer grows further, Q decreases monotonically. At $Fo = 1200$, Q is reduced by about 30% of its value at $Fo = Fo_{tr}$. Note that Q includes both latent heat transfer due to phase change and apparent heat transfer from the ambient. In Fig. 4(b) ($T_c^* = 253$ K), Q at $Fo = 1200$ is about 50% of its value at $Fo = Fo_{tr}$. This indicates that, under the same ambient conditions (T_∞, u_∞ and W_∞), the phase change effect is weaker for the low cold plate temperature. On the other hand, the reduction in heat transfer (including both latent and apparent heat) due to frost build-up is more significant for the cold plate at a lower surface temperature.

3.3. *Comparison of the prediction with the experimental data*

The accurate measurement of the temperature and frost density within the frost layer is a very difficult

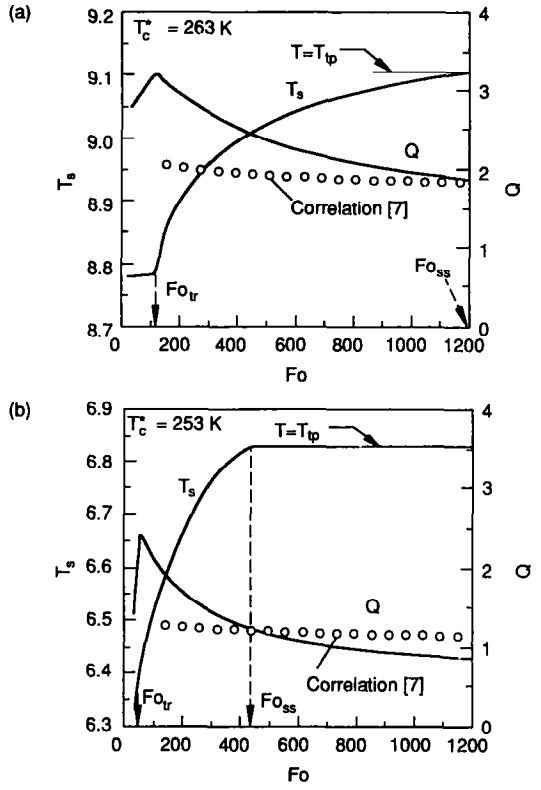

FIG. 4. Time variations of the temperature and dimensionless heat flux for (a) $T_c^* = 263$ K; and (b) $T_c^* = 253$ K.

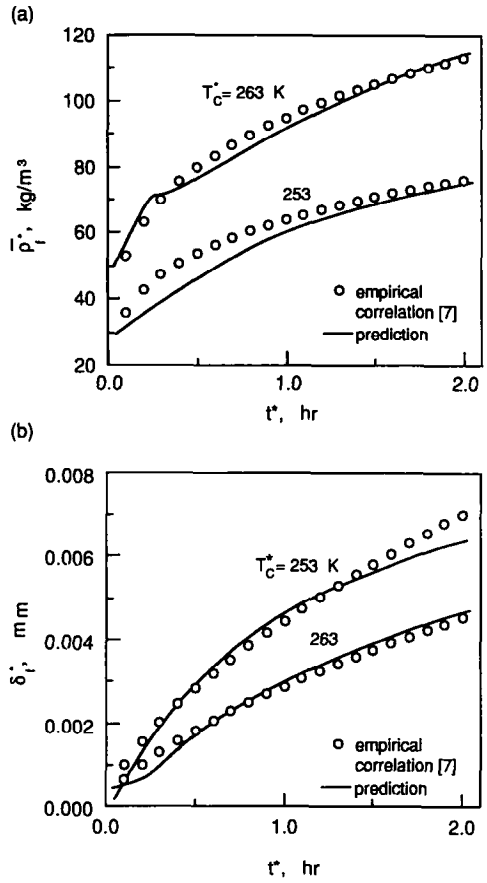

FIG. 5. Comparison with the experimental data: (a) the average frost density; and (b) frost thickness.

task. To date, no data are available in the literature which give a quantitative description of these distributions as a function of time. The most reliable data taken from the experiments are usually those for the average frost density and thickness. In an experimental study [7], a series of tests was performed to measure the average frost density and thickness as a function of time and ambient conditions. The comprehensive correlations that describe the relations between the frost properties and ambient parameters (such as Reynolds number, humidity ratio, etc.) were developed (see the Appendix). In Fig. 5, the results taken from these empirical correlations are compared with the predictions obtained in this study. Good agreement between the measured and predicted $\bar{\rho}_f^*$ and δ_f^* has been achieved for $T_c^* = 263$ K (with the diffusion factor, $F = 3$; see equation (16)). For $T_c^* = 253$ K ($F = 0.11$), some deviation at the later stage of frost growth (the quasi-steady state) in δ_f^* exists. This may be in part due to the uncertainty associated with empirical correlations, which are slightly outside the applicable range of $-15°C < T_c^* < -5°C$.

In Fig. 4, the measured heat flux is also compared with the prediction. The predicted heat flux, normalized with the convective heat transfer (equations (43) and (44)), agrees well with the measured one for the quasi-steady state. At the early stage, the prediction is higher than the experimental data. This is partly due to the extrapolation of the correlations to the initial growth stage and partly because of the simplicity of the early growth model.

3.4. *Effective mass diffusivity of frost*

The effect of F on the prediction of the frost properties is investigated by assuming different values and comparing the results with the measured frost thickness and average frost density. In Fig. 6(a), the numerical results of the average frost density, frost thickness and frost surface temperature are shown for different F values under the same ambient and cold plate boundary conditions. It can be seen that an increase in F results in an increase in the predicted $\bar{\rho}_f$, but it has a less significant effect on δ_f, and it will cause the surface temperature of the frost layer, T_s, to reach T_{tp} at a later time. (The best agreement with the experimental results is, in this example, achieved for $F = 3$ for $T_c^* = 263$ K, a result that is consistent with measurements of water vapor diffusion in snow [12, 14]; these data indicate F ranging from 2.2 to 3.5 for a snow temperature of 264–272 K.) This further suggests that the accurate determination of the frost surface temperature may help indirectly to confirm the significance of F in modeling the frost growth and densification.

Similar calculations are also performed for different

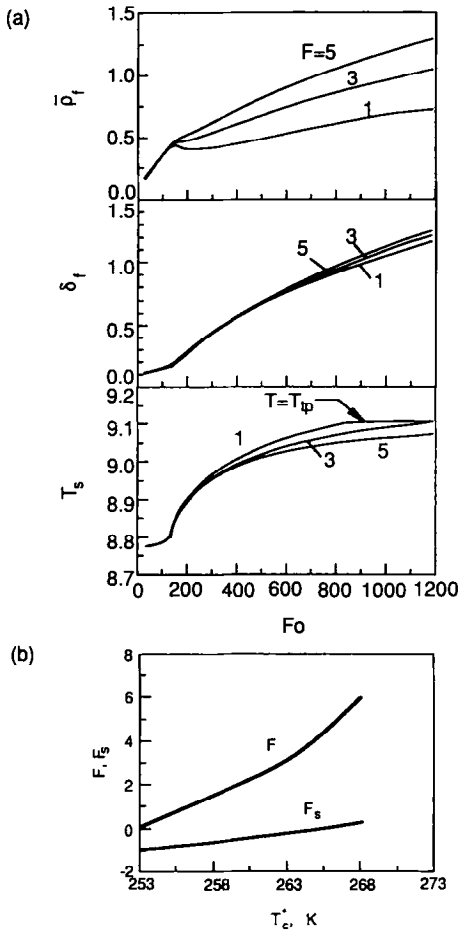

FIG. 6. (a) Effects of F and F_s on the prediction for the average density, thickness and surface temperature of the frost layer: $T_c^* = 263$ K; and (b) diffusion factors as a function of T_c^*.

cold plate temperatures to find a qualitative relation of F, using the empirical correlations as a guide. Figure 6(b) shows the diffusion factors, F (internal) and F_s (at the frost surface) as a function of T_c^*. It can be seen that, based on the experimental data, F increases as the cold plate temperature increases within the range of T_c^* shown in Fig. 5; the model is not applied for $T_c^* > 268$ K because experimental observations indicate no frost cover when $T_\infty^* = 293$ K and $T_c^* > 268$ K [7]. Also, F is always positive or for very cold temperatures perhaps near zero, while F_s is negative for $T_c^* < 266$ K. This means that, for $T_c^* > 253$ K and $T_\infty^* = 293$ K, the total effective mass diffusivity within the frost layer, D_{eff}^*, is larger than the effective diffusivity which only accounts for molecular diffusion ($=\varepsilon_\gamma D^*$). On the other hand, the effective diffusivity at the interface between the frost and ambient is less than the value $\varepsilon_\gamma D^*$. This is generally expected, since, for diffusion from a plain medium to a porous medium, the diffusion resistance, due to geometrical change, causes the effective diffusivity to be less than that for molecular diffusion, i.e. the tortuosity factor, $1/(1+F_s)$, is greater than 1, as known in the diffusion processes in porous media with fixed matrices [19]. The difference between internal transport properties and interfacial properties (effective diffusivity, thermal conductivity, etc.), emerging from the volumetric averaging formulation, is a topic that has drawn a lot of attention recently [20, 21]. But for the frost problem (moving boundary problem), no analysis has been made yet.

It is noted that F_s mainly influences the prediction of δ_f (equation (17)) while F effects ε_{ff} (i.e. the internal densification). The theoretical determination of F (or F_s) is a difficult task but may be possible if a proper structural model for the frost layer is constructed, as demonstrated in ref. [22] where the porous matrix is fixed. However, even in that case [22], only a very simple periodic structural model was used. For a frost layer, the time variation of the structural characteristics needs to be considered. At this time, we only point out that the non-homogeneity in the frost pore size at the microscopic level, resulting from simultaneous heat and mass transfer and phase change, causes an enhancement in the local diffusion flux, which may be, along with frost metamorphism, responsible for the local frost densification in addition to the main stream diffusion along the coordinate direction. This phenomenon, when described on a one-dimensional, macroscopic basis, can be expressed by a local effective mass diffusivity which is larger than $\varepsilon_\gamma D^*$ (i.e. $F > 0$). This conclusion, although no direct comparison can be made, is supported by a microscopic study of water vapor transport in an assumed two-dimensional ice crystal lattice, which simulates snow metamorphism under a temperature gradient, by Christon *et al.* [23]. Their reported results show that the ratio of the effective diffusivity to the water vapor–air binary diffusivity, as a function of temperature and area (of the lattice) ratio, is between 1.9 and 2.5 for a temperature of 263–273 K and an area ratio of 0.1–0.5. This ratio is translated in our case to an F to be approximately 1–2.

4. SUMMARY

This study presents a new frost growth model that predicts a complete process of frost growth on a flat plate for given ambient conditions and cold plate temperature. Both spatial and temporal variations of temperature, frost density and rate of densification can be predicted, along with the time variation of frost thickness, provided that the proper transport properties are used. Guided by experimental data, it is found that the internal frost densification can be described by using an effective mass diffusivity that accounts for the deviation of actual mass transport phenomenon from Fick's diffusion. For a cold temperature of 267 K, the results shown that the effective mass diffusivity for internal densification is up to seven times larger than the counterpart for molecular diffusion of water vapor in air, while the opposite is

true for interfacial effective diffusivity. These results compare well with the independent measurements of effective mass diffusivity of water vapor in snow for a temperature range of 264–272 K.

REFERENCES

1. D. L. O'Neal and D. R. Tree, A review of frost formation in simple geometries, *ASHRAE Trans.* **91,** 267 (1985).
2. M. M. Padki, S. A. Sherif and R. M. Nelson, A simple method for modeling the frost formation phenomenon in different geometries, *ASHRAE Trans.* **95,** 1127–1137 (1989).
3. S. M. Sami and T. Duong, Mass and heat transfer during frost growth, *ASHRAE Trans.* **95,** 158–165 (1989).
4. P. L. T. Brian, R. C. Reid and Y. T. Shah, Frost deposition on cold surfaces, *Ind. Engng Chem. Fundam.* **9,** 275–280 (1970).
5. C. J. Cremers and O. J. Hahn, Frost density measurements on vertical cylinders by gamma-ray attenuation, *Adv. Cryogen. Engng* **23,** 371–375 (1978).
6. Y. Hayashi, A. Aoki, S. Adachi and K. Hori, Study of frost properties correlating with frost formation types, *J. Heat Transfer* **99,** 239–245 (1977).
7. Y. Mao, R. W. Besant and K. S. Rezkallah, Measurement and correlations of frost properties with air flow over a flat plate, *ASHRAE Trans.* (in press).
8. S. Whitaker, Simultaneous heat, mass and momentum transfer in porous media: a theory of drying. In *Advanced in Heat Transfer* (Edited by J. P. Hartnett and T. F. Irvine, Jr.), Vol. 13, pp. 119–203. Academic Press, New York (1977).
9. Y.-X. Tao, R. W. Besant and K. S. Rezkallah, Unsteady heat and mass transfer with phase change in an insulation slab: frosting effects, *Int. J. Heat Mass Transfer* **34,** 1593–1603 (1991).
10. T. Y. Bong, N. E. Wijeysundera, E. L. Saw and K. O. Lau, Comparison of beta-ray and gamma-ray transmission methods for measurement of frost density distribution, *Exp. Thermal Fluid Sci.* **4,** 567–576 (1991).
11. J. D. Yonko and C. F. Sepsy, An investigation of the thermal conductivity of frost while forming on a flat horizontal plate, *ASHRAE Trans.* **73,** 11 (1967).
12. Y. C. Yen, Recent studies in snow properties. In *Advances in Hydrosciences* (Edited by V. T. Chow), Vol. 5, pp. 173–213. Academic Press, New York (1969).
13. D. H. Male, The seasonal snowcover. In *Dynamics in Snow and Ice Mass* (Edited by S. C. Colbeck), pp. 305–395. Academic Press, New York (1980).
14. Z. Yosida, Heat transfer by water vapor in snow cover, *Low Temp. Sci.* **5,** 93–100 (1950).
15. Y.-X. Tao and M. Kaviany, Simultaneous heat and mass transfer from a two-dimensional, partially liquid covered surface, *J. Heat Transfer* **113,** 874–882 (1991).
16. W. M. Kays and M. E. Crawford, *Convective Heat and Mass Transfer*, p. 217. McGraw-Hill, New York (1980).
17. F. P. Incropera and D. P. DeWitt, *Fundamentals of Heat Transfer*, p. 285. Wiley, New York (1985).
18. P. Griffith, Dropwise condensation. In *Handbook of Heat Transfer: Fundamentals* (Edited by W. M. Rohsenow, J. P. Hartnett and E. N. Ganić), Section 11, Part 2. McGraw-Hill, New York (1985).
19. F. A. L. Dullien, *Porous Media: Fluid Transport and Pore Structure*, p. 225. Academic Press, New York (1979).
20. M. Kaviany, *Principles of Heat Transfer in Porous Media*, pp. 141–148. Springer, New York (1991).
21. M. Prat, On the boundary conditions at the macroscopic level, *Transp. Porous Media* **4,** 259–280 (1989).
22. D. Ryan, R. G. Carbonell and S. Whitaker, Effective diffusivities for catalyst pellets under reactive conditions, *Chem. Engng Sci.* **35,** 10–16 (1980).
23. M. Christon, P. Burns and R. Sommerfeld, A 2-D microscopic simulation of heat and mass transport in dry snow, *Chem. Engng Commun.* **87,** 87–105 (1990).

APPENDIX

The following empirical correlations were reported in ref. [7]:

frost thickness

$$\frac{\delta_f^*}{[\mathrm{m}]} = 0.156\left(\frac{x}{d_H}\right)^{-0.098} W_\infty^{1.723} T'^{1.100} Re_{d_H}^{0.343} Fo_{d_H}^{0.655}$$

average frost density

$$\frac{\rho_f^*}{\rho_\beta^*} = 5.559\times 10^{-6}\left(\frac{x}{d_H}\right)^{-0.137} W_\infty^{-0.413} T'^{-0.997} \times Re_{d_H}^{0.715} Fo_{d_H}^{0.252}$$

where d_H is the hydraulic diameter characterizing the ambient, internal, forced convective flow, Fo_{d_H} is defined using the air properties, and $T' = T_{tp} - T_c$. The applicable range of the above relations is

$$-15^\circ\mathrm{C} \leqslant T_c^* \leqslant -5^\circ\mathrm{C}, \quad 3\times 10^3 \leqslant Re_{d_H} \leqslant 7\times 10^3$$

$$13 \leqslant Fo_{d_H} \leqslant 104, \quad 0.004 \leqslant W_\infty \leqslant 0.01.$$